

Milliarcsecond-Scale Structure in the Gamma-Ray Loud Quasar PKS 1622–297

Kiyoaki WAJIMA¹, Hayley E. BIGNALL², Hideyuki KOBAYASHI^{3,4}, Hisashi HIRABAYASHI^{5,6},
Yasuhiro MURATA^{5,6}, Philip G. EDWARDS^{5,6}, Masato TSUBOI^{4,7,8}, and Kenta FUJISAWA⁹

¹*Korea Astronomy and Space Science Institute, 61-1 Hwaam-dong, Yuseong, Daejeon 305-348, Korea*
kiyoaki@trao.re.kr

²*Joint Institute for VLBI in Europe, Postbus 2, NL-7990 AA Dwingeloo, The Netherlands*

³*National Astronomical Observatory of Japan, 2-21-1 Osawa, Mitaka, Tokyo 181-8588*

⁴*Department of Astronomy, School of Science, The University of Tokyo, 7-3-1 Hongo, Bunkyo, Tokyo 113-0033*

⁵*Institute of Space and Astronautical Science, Japan Aerospace Exploration Agency,
3-1-1 Yoshinodai, Sagami-hara, Kanagawa 229-8510*

⁶*Department of Space and Astronautical Science, The Graduate University for Advanced Studies,
3-1-1 Yoshinodai, Sagami-hara, Kanagawa 229-8510*

⁷*Nobeyama Radio Observatory, Minamimaki, Minamisaku, Nagano 384-1305*

⁸*Department of Astronomical Science, The Graduate University for Advanced Studies,
2-21-1 Osawa, Mitaka, Tokyo 181-8588*

⁹*Department of Physics, Faculty of Science, Yamaguchi University,
1667-1 Yoshida, Yamaguchi, Yamaguchi 753-8512*

(Received 2005 July 13; accepted 2005 October 23)

Abstract

We have made a high-resolution VLBI observation of the gamma-ray loud quasar PKS 1622–297 with the HALCA spacecraft and ground radio telescopes at 5 GHz in 1998 February, almost three years after the source exhibited a spectacular GeV gamma-ray flare. The source shows an elongated structure toward the west on the parsec scale. The visibility data are well modeled by three distinct components; a bright core and two weaker jet components. Comparison with previous observations confirms that the jet components have an apparent superluminal motion up to $12.1 h^{-1}c$, with the inner jet components having lower superluminal speeds. We apply the inverse Compton catastrophe model and derive a Doppler factor, δ , of 2.45, which is somewhat lower than that of other gamma-ray loud active galactic nuclei (AGNs), suggesting the source was in a more quiescent phase at the epoch of our observation. As an alternative probe of the sub-parsec scale structure, we also present the results from multi-epoch ATCA total flux monitoring, which indicate the presence of persistent intraday variability consistent with refractive interstellar scintillation. We examine the gamma-ray emission mechanism in the light of these observations.

Key words: galaxies: active — galaxies: jets — galaxies: quasars: individual (PKS 1622–297) — ISM: general — techniques: interferometric

1. Introduction

Observations made with the EGRET (Energetic Gamma Ray Experiment Telescope) gamma-ray detector onboard the CGRO (Compton Gamma Ray Observatory) spacecraft resulted in the identification of nearly 70 gamma-ray emitting AGNs (Hartman et al. 1999), with more recent studies increasing the number of EGRET sources with at least one plausible AGN association by ~ 50 (Sowards-Emmerd et al. 2003, 2004). These are predominantly radio-loud AGNs, which suggests a strong connection between the gamma-ray emission and the radio emission.

Recent VLBI observations have revealed several interesting features of the parsec-scale structures in gamma-ray loud AGNs. Jorstad et al. (2001a) completed multi-epoch VLBA (Very Long Baseline Array) observations of 42 gamma-ray loud AGNs at 22.2 and 43.2 GHz, and oc-

asionally 8.4 and 15.4 GHz. From these they found that 10 gamma-ray flares in eight objects fall within 1σ uncertainties of extrapolated epoch of zero separation from the core of a superluminal radio component. In addition they compared their observations with variability of polarized radio flux and gamma-ray flares, and suggest that gamma-ray emission occurs in the superluminal radio components (Jorstad et al. 2001b). The fact that the gamma-ray flare occurs close to the time of the maximum polarized radio flux density and after the mm-wavelength radio flare favors a model in which the gamma-ray emission is produced by inverse Compton scattering by the electrons in the parsec-scale jet rather than closer to the central engine.

Gamma-ray emission from inverse Compton scattering (e.g. Sikora et al. 1994) requires a smaller jet viewing angle and higher Doppler factor because the emission should be concentrated in the jet direction. Jiang, Cao, and

Hong (1998) compiled the published data for 52 AGNs (including 18 EGRET AGNs), for which measurements of the angular size and radio flux density of the VLBI core, proper motion of the components in the jet, and X-ray flux density were available. They applied the inhomogeneous jet model of Königl (1981) to the sample and showed that the derived mean viewing angle for 14 EGRET sources is 4.9° and the Doppler factors of these sources are greater than 4.7. These results also indirectly support the gamma-ray emission model by inverse Compton scattering. However, there are still large uncertainties for the derived parameters in gamma-ray loud AGNs and it is therefore important to verify the milliarc-second (mas)-scale properties for individual sources precisely by VLBI observations.

In this paper we report the results of an observation of PKS 1622–297 (J1626–2951) by VSOP (VLBI Space Observatory Programme), consisting of the radio-astronomy spacecraft HALCA and ground radio telescopes located around the world (Hirabayashi et al. 1998). VSOP observations enable improvement of the angular resolution by up to a factor of three compared to ground-only VLBI observations at the same frequencies.

PKS 1622–297 is one of the gamma-ray emitting sources with a high-confidence identification by EGRET (Hartman et al. 1999). During an outburst at epoch 1995.48, the source was the most luminous gamma-ray emitting AGN ever detected and showed rapid gamma-ray variability by a factor of at least 3.6 in less than 7.1 hours (Mattox et al. 1997). It is a strong, compact radio source optically identified as a quasar (Saikia et al. 1987; Stickel et al. 1994) with a fractional polarization of more than 4% at cm-wavelengths (Tabara, Inoue 1980; Impey, Tapia 1990). Previous results of VLBI observations are described by Tingay, Murphy, and Edwards (1998), Fomalont et al. (2000), Jorstad et al. (2001a), and Tingay et al. (2002).

PKS 1622–297 has also been reported to display intraday variability (IDV) at 8.6 GHz at two epochs in 1994 (Kedziora-Chudczer et al. 2001). Both intrinsic and extrinsic origins have been suggested for IDV (Wagner, Witzel 1995), while current radio observations show that interstellar scintillation (ISS) is mainly responsible for the rapid IDV feature, such as the annual modulation in the scintillation timescale (Rickett et al. 2001; Jauncey, Macquart 2001; Bignall et al. 2003b), and detection of time delay across the 10,000 km baseline between ATCA and VLA (Jauncey et al. 2003). Both intrinsic and extrinsic explanations require very compact source structure. We present here the results of multi-frequency multi-epoch monitoring of PKS 1622–297 with the Australia Telescope Compact Array (ATCA) and discuss the origin of the IDV, and consider the gamma-ray emission mechanism based on both the VSOP and ATCA observations.

A redshift of $z = 0.815$ was listed in Wright and Otrupcek (1990), corresponding to an angular-to-linear scale conversion of $5.3 h^{-1} \text{pc mas}^{-1}$ assuming a Hubble constant, H_0 , of $100 h \text{ km s}^{-1} \text{ Mpc}^{-1}$, a flat universe with a cosmological constant, $\Omega_\Lambda = 0.7$, and a pressureless

matter density parameter, $\Omega_m = 0.3$ (Balbi et al. 2000). However, this redshift has been questioned (Jackson et al. 2002), and so although we adopt it in this paper, it should be kept in mind that confirmation of this value is required.

The details of the observations and data reduction are described and the results are presented in section 2 and 3 for VSOP and ATCA observations, respectively. In section 4, we discuss the mas-scale structure and the gamma-ray emission mechanism in the light of these observations. Throughout this paper, we define the spectral index, α , as $S_\nu \propto \nu^\alpha$.

2. VSOP Observation

2.1. Observation and Data Reduction

The VSOP observation was made in left-circular polarization at 5 GHz on 1998 February 22, as a part of the VSOP AGN Survey Program (Hirabayashi et al. 2000). The ground radio telescopes were Hartebeesthoek 26 m (South Africa), Hobart 26 m (Australia), and Shanghai 25 m (China). Data from HALCA were transferred via the Tidbinbilla (Australia) tracking station. The data were correlated at the Dominion Radio Astrophysical Observatory S2 correlator (Carlson et al. 1999) in Penticton (Canada). Output pre-averaging time were 0.1 second for space-ground baselines and 2 seconds for ground-ground baselines, respectively. The observation bandwidth was 32 MHz and the total observing time was 4.5 hours.

We carried out post-processing of the correlated data using the Astronomical Image Processing System (AIPS) software developed by the National Radio Astronomy Observatory (NRAO) and the Caltech software Difmap (Shepherd 1997). We applied *a priori* amplitude calibration using the antenna gain factors and system noise temperature measurements. For fringe-fitting, we used a solution interval of three minutes and a point-source model, with Shanghai serving as the reference telescope. We detected fringes on all ground-ground baselines. On the space-ground baselines, however, we could detect significant fringes only within an hour from the beginning of the observation, corresponding to the shorter space baselines, and so we excluded the HALCA data after that time.

We exported the fringe-fitted visibility data to Difmap for imaging. At first we integrated the data over 10 seconds to reconcile the different preaveraging time from the correlator output, and performed several iterations of cleaning and self-calibration to the phases. To ensure a better angular resolution with the HALCA data, we adopted uniform weighting of the data with gridding weights scaled by amplitude errors raised to the power of -1 (Hirabayashi et al. 2000). Figure 1 shows the (u, v) coverage of all baseline pairs for the times that fringes were successfully detected. The elliptical tracks represent the baselines between ground stations, while space-ground baselines contribute to the approximately linear inner and outer tracks. The longest baseline of the observation is 17,000 km, corresponding to 1.3 times the Earth's diame-

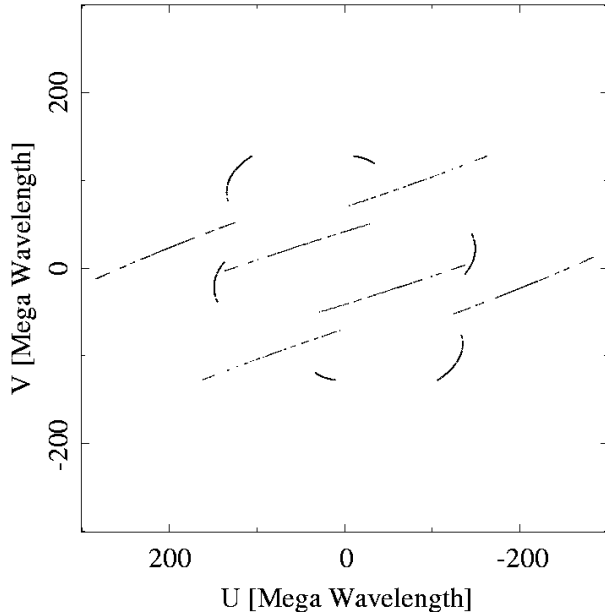


Fig. 1. (u, v) coverage for the VSOP observation of PKS 1622–297 at epoch 1998.15 (1998 February 22).

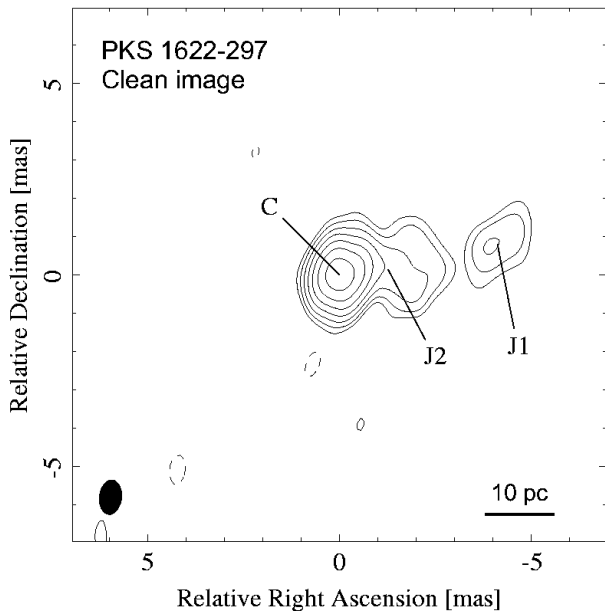


Fig. 2. 5 GHz VSOP image of PKS 1622–297 at epoch 1998.15 (1998 February 22). The restoring beam is $0.91 \text{ mas} \times 0.58 \text{ mas}$ at a position angle of 7° , which is indicated at the lower left corner. Contour levels are $9.5 \times (-1, 1, 2, 4, \dots, \text{and } 64) \text{ mJy beam}^{-1}$, and the peak flux density is $0.84 \text{ Jy beam}^{-1}$. The labels show the Gaussian model fitting components. See table 1 for detailed parameters.

ter.

2.2. VSOP Results

Figure 2 shows the image of PKS 1622–297. We detect three components, which are the bright core, C, a moderately bright jet component, J2, 1.3 mas from the

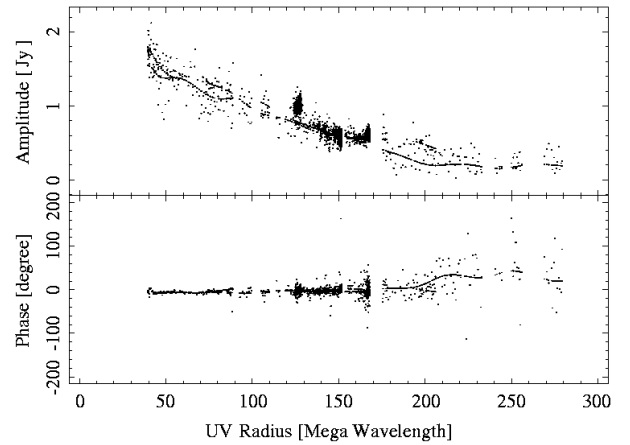


Fig. 3. Calibrated visibility amplitudes (top) in Jy and phases (bottom) in degree as a function of the (u, v) distance. Dotted lines show the clean component model used for restoring the image in figure 2.

core, and a weak jet component, J1, 4.2 mas from the core. The jet extends to the west, which is consistent with previous results (Tingay et al. 1998; Fomalont et al. 2000; Jorstad et al. 2001a; Tingay et al. 2002). However we did not detect the stationary component ~ 15 mas from the core, which was detected by Tingay, Murphy, and Edwards (1998) and Fomalont et al. (2000) at 5 GHz, and Jorstad et al. (2001a) at 15 GHz. This component is relatively faint in the 5 GHz observation (Tingay et al. 1998) and even weaker ($\sim 30 \text{ mJy}$) in the 15 GHz observations (Jorstad et al. 2001a). The flux density of the component at 5 GHz was 50 mJy at epoch 1994.64 (Tingay et al. 1998) and 40 mJy at epoch 1996.43 (Fomalont et al. 2000). The upper limit of the component on our image at epoch 1998.15 is 20 mJy , which corresponds to the 7σ detection limit. Although it is likely that the component is resolved, the sparse (u, v) coverage of our observation may result in a dynamic range that is not adequate to detect the component.

Figure 3 shows the calibrated visibility amplitudes and phases as a function of (u, v) distance. The clustered visibilities in the range between $120 \text{ M}\lambda$ and $170 \text{ M}\lambda$ are the ground-ground baseline data, while the space-ground visibilities are widely distributed up to $280 \text{ M}\lambda$. The space-ground visibilities show that the source is clearly resolved. We could not detect significant fringes on baselines longer than $280 \text{ M}\lambda$, indicating that the source is being resolved out on those baselines.

The shortest baselines sampled in the observation are $\sim 40 \text{ M}\lambda$, as shown in figure 3. PKS 1622–297 was fortuitously observed one week earlier as part of the multi-epoch ATCA monitoring of VSOP Survey Program sources, yielding flux densities on the ATCA 6 km baseline of 2.33 Jy at 1.384 GHz , 2.23 Jy at 2.496 GHz , 2.41 Jy at 4.800 GHz , and 2.49 Jy at 8.640 GHz (Tingay et al. 2003). A single-dish measurement from the University of Michigan Radio Astronomy Observatory (UMRAO) gave an 8.0 GHz flux density of the source of

2.49 ± 0.06 Jy on 1998 February 28, in excellent agreement with the ATCA value. The spectral index between 4.8 and 8.6 GHz at this epoch was comparatively flat, $\alpha \sim 0.1$: Figure 2 of Tingay et al. (2003) reveals that the spectrum was more inverted earlier and later in the monitoring program. The contemporaneous flux density measurement is consistent with a simple extrapolation of our correlated flux density to smaller baselines. We also examined our amplitude calibration using `gscale` in Difmap and resulted in correction factors of less than 10% for all stations. We therefore believe the amplitude calibration of our observation to be reliable.

2.3. Model Fitting and Proper Motion of Each Component

To quantify the size and relative location of components, we modeled the calibrated visibility data with elliptical Gaussian components. Table 1 gives the model fitting results and the position of each component is indicated in figure 2. We performed the model fitting using the task ‘IMFIT’ in AIPS.

The data were modeled satisfactorily by three distinct components. The brightest component, labeled C, is the brightest and most compact, consistent with it being the core. Weaker components, labeled J2 and J1, are situated to the west of the core. We compared the positions of each component with those measured by Jorstad et al. (2001a). Figure 4 shows the distance of each component from the core as a function of observed epoch. The results of a least-squares linear fit for each component are also plotted as dashed lines on figure 4. Component J2 can be identified with the B1+D1+E2 of Jorstad et al. (2001a), and J1 with their component F2. Tingay et al. (2002) have obtained an image of PKS 1622–297 with VSOP at a different epoch from ours and detected a weak jet component toward the west approximately 1.5 mas from the core. Although they do not apply model fitting to this component, they mention that it is likely to be component B1+D1+E2. Our results clearly show that these two components are identical.

Jorstad et al. (2001a) have also detected the component F1, as shown in figure 4. F1’s position was less well-defined, and its motion appeared to be much slower than that of F2. Extrapolating the motion of F1 suggests it would be located 5.6 ± 0.5 mas from the core at the epoch of our VSOP observation. This position is slightly beyond the northwestern extension of J1 (see figure 2), and so it is possible that J1 may be a blended component of F2 and F1.

We could not detect the component that corresponds to B2+D2+E3 detected by Jorstad et al. (2001a). If we assume a linear motion of B2+D2+E3, we would detect the component with ~ 0.4 mas separation from the core. While there is emission evident at this location in figure 2, it is adequately represented by our model fits for components C and J2. Our non-detection may be due to insufficient angular resolution. However, we point out that Tingay et al. (2002) also did not detect this component in their VSOP image at epoch 2000.32. Their observa-

tion had better angular resolution than ours and suggests that B2+D2+E3 has either faded away or has a significantly different speed than that determined by Jorstad et al. (2001a).

Apparent proper motions of $\mu = 0.13 \pm 0.01$ (for B2+D2+E3), 0.34 ± 0.02 (for J2), and 0.70 ± 0.11 (for J1) correspond to apparent velocities of $(2.2 \pm 0.2) h^{-1}$, $(5.9 \pm 0.3) h^{-1}$, and $(12.1 \pm 1.9) h^{-1}$, respectively (see also table 2). The ejection epochs listed in table 2 are derived by extrapolating the linear relations of each component. The ejection epoch of J1 is estimated to be 1992.39 ± 0.73 . This is coincident with a local maximum in the gamma-ray emission at 1991.95 although there is a relatively large error. Although the gamma-ray light curve is under-sampled, the coincidence suggests a close relationship between gamma-ray emission and ejection of a new jet component.

Jorstad et al. (2001a) pointed out that inner components have superluminal speeds but they are lower than those of outer components. The apparent speed of J2 is half that of J1 and our result, combining with results by Jorstad et al. (2001a), confirms this tendency. We will discuss features of each component derived from β_{app} and the Doppler factor in section 4.1.

3. ATCA Observations

3.1. Observation and Data Reduction

PKS 1622–297 was included in a sample of 118 compact, flat-spectrum AGN observed at two-epochs and four frequencies with ATCA as part of survey for sources displaying IDV (Kedziora-Chudczer et al. 2001). Twenty-two sources (19% of the sample) were found to display significant IDV at at least one frequency and at least one epoch, with significant IDV observed for PKS 1622–297 at 8.6 GHz at both epochs. This led to the inclusion of PKS 1622–297 in the sample of 21 sources monitored with the ATCA by Bignall (2003a).

PKS 1622–297 was monitored at 4.8 GHz and 8.64 GHz at ten epochs between 2001 February 4 and 2002 February 21. The observing technique and data reduction methods are described in detail in Bignall et al. (2003b); briefly, observations at each epoch were generally made over a two-day period. Sources were observed in scans of up to 5 minutes every ~ 1 hour while they were above an elevation of 15° . A number of calibrator sources were included in the observing schedule and observed in a similar manner.

The data were reduced in MIRIAD (Sault et al. 1995). Time-dependent antenna gain corrections were derived at each frequency from observations of the calibrators, and found to vary by $\lesssim 1\%$ over each epoch. After applying these gain corrections, averaged over 30–60 minutes and linearly interpolated, phase self-calibration was performed using a point source model and 10 second integrations. The real parts of the visibilities for Stokes parameters I , Q , and U were averaged over intervals of several minutes.

Table 1. Model fitting results.

Component	S^* (Jy)	r^\dagger (mas)	ϕ^\ddagger (deg)	θ_{maj}^\S (mas)	$\theta_{\text{min}}^\parallel$ (mas)	P.A.# (deg)	T_B^{**} (10^{11} K)
C	1.50 ± 0.01	0	0	0.71 ± 0.01	0.54 ± 0.01	-78.9 ± 1.7	3.73 ± 0.07
J2	0.34 ± 0.02	1.31 ± 0.05	-81.2 ± 2.3	2.09 ± 0.08	1.05 ± 0.07	69.1 ± 2.8	0.15 ± 0.01
J1	0.13 ± 0.01	4.28 ± 0.07	-78.1 ± 0.9	1.58 ± 0.12	0.69 ± 0.12	-50.7 ± 5.1	0.11 ± 0.02

Notes.

* Flux density of each component.

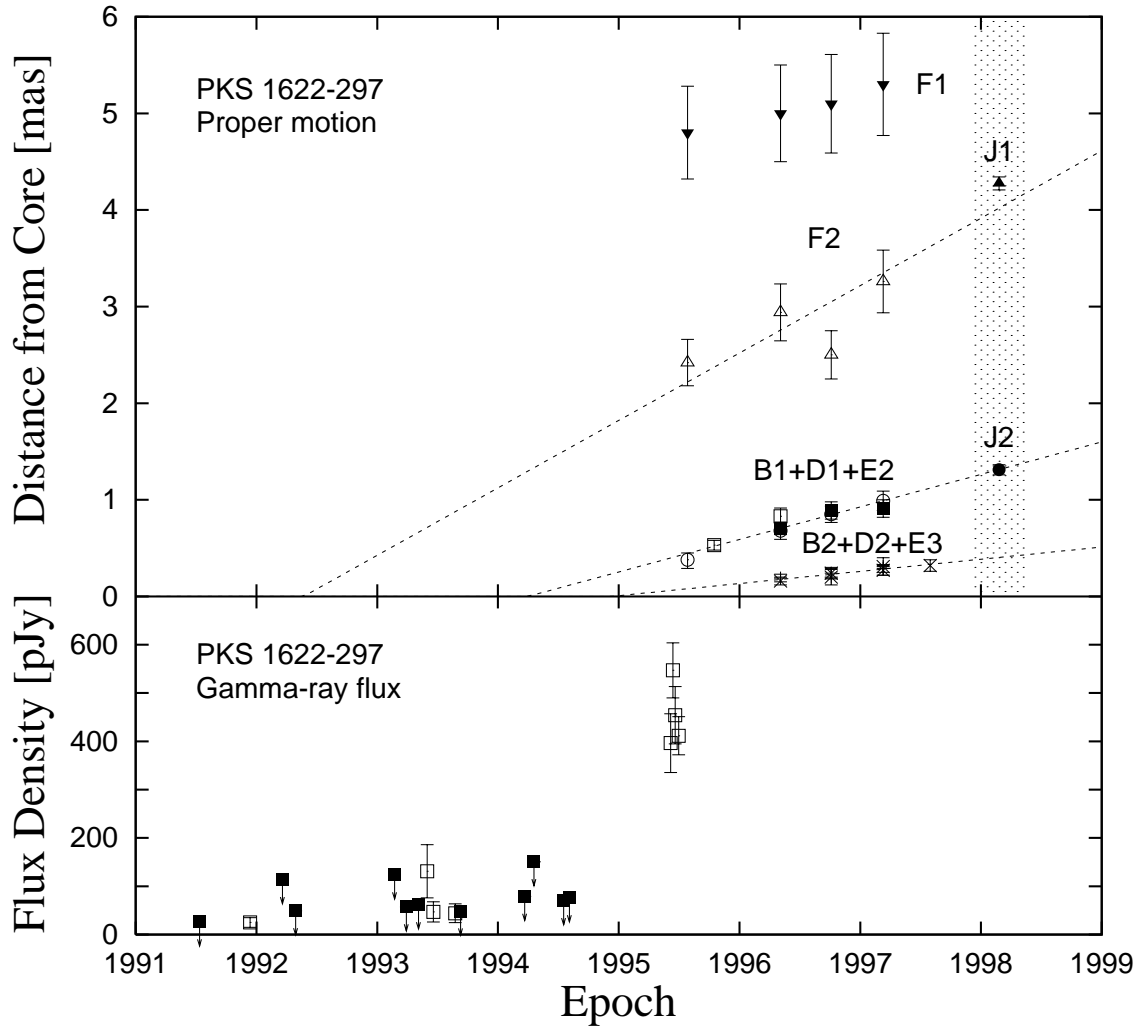
 \dagger Distance of each component from the origin defined by component C. \ddagger Position angle of each component with respect to the origin (east of north). $\S, \parallel, \#$ Parameters of Gaussian model: major and minor axes in mas (FWHM) and the position angle (P.A.) of the major axis.** Peak brightness temperature given in the rest frame of the host galaxy (assuming $z = 0.815$; see section 1).

Fig. 4. (Top) Distance of components from the core as a function of observed epoch. The measurements in 1998.15 (J1 and J2) are our results. See table 2 for numerical values. The data before 1997.58 (B2+D2+E3, B1+D1+E2, F2, and F1) are from Jorstad et al. (2001a). The dashed lines show results of a least-squares linear fit. Position uncertainties are not listed for some data points in Jorstad et al. (2001a), and we therefore assume the uncertainties as 10% of listed values. (Bottom) Gamma-ray light curve in picoJy observed by EGRET (Hartman et al. 1999). Open and filled squares show the positive and marginal (or non-) detections, respectively. Upper limits are plotted in the latter case.

Table 2. Apparent proper motion of each component.

Component	Proper motion (mas yr ⁻¹)	Apparent velocity	Ejection epoch (yr)
B2+D2+E3	0.13 ± 0.01	(2.2 ± 0.2) <i>h</i> ⁻¹ <i>c</i>	1994.94 ± 0.08
B1+D1+E2, J2	0.34 ± 0.02	(5.9 ± 0.3) <i>h</i> ⁻¹ <i>c</i>	1994.25 ± 0.10
F2, J1	0.70 ± 0.11	(12.1 ± 1.9) <i>h</i> ⁻¹ <i>c</i>	1992.39 ± 0.73

Table 3. ATCA monitoring results.

Epoch	Time span (days)	$N_{4.8}$	$S_{4.8}$ (Jy)	$m_{4.8}^*$ (%)	$S_{\max}^{4.8} - S_{\min}^{4.8}$ (Jy)	$N_{8.6}$	$S_{8.6}$ (Jy)	$m_{8.6}^\dagger$ (%)	$S_{\max}^{8.6} - S_{\min}^{8.6}$ (Jy)
2001 Feb 4	2.77	24	2.78	1.4	0.12	25	2.76	1.8	0.15
2001 Mar 17	1.96	26	2.90	0.6	0.06	26	2.71	0.8	0.07
2001 Apr 6	1.96	23	3.02	0.9	0.08	23	2.70	3.7	0.25
2001 Jun 2	1.42	22	2.58	3.8	0.32	22	2.28	3.9	0.28
2001 Aug 4	0.86	9	2.59	1.2	0.09	9	2.13	0.7	0.04
2001 Aug 11	1.15	15	2.43	1.2	0.08	15	2.14	0.9	0.06
2001 Sep 20	2.12	25	2.51	2.3	0.21	24	2.26	3.2	0.26
2001 Nov 29	1.45	20	2.88	0.7	0.07	20	2.62	1.2	0.13
2002 Jan 4	1.97	21	2.76	0.4	0.04	21	2.52	1.6	0.12
2002 Feb 21	2.07	10	2.83	1.6	0.13	10	2.33	1.7	0.14

*, † We expect to see rms variations up to 0.5% as a result of measurement uncertainties.

3.2. ATCA Results

The results of the ATCA monitoring are given in table 3. At each epoch, the time spanned by the observations of PKS 1622–297 is given, together with the number of measurements (N ; usually the same at 4.8 and 8.6 GHz), the mean flux density (\bar{S}), the modulation index ($m = 100\sigma_S/\bar{S}$), and the range of the measured flux densities ($S_{\max} - S_{\min}$), at each frequency. The results are shown graphically in figure 5. The upper and lower panels of figure 5 show the observation on 2001 June 2 – 3, when the largest amplitude IDV was observed ($S_{\max} - S_{\min} \sim 0.3$ Jy), and long-term flux variation, respectively. Variations at a level exceeding that expected from measurement uncertainties are seen at both frequencies at all epochs, with formally significant evidence of IDV present at at least one frequency at almost all epochs, whereas Kedziora-Chudczer et al. (2001) had succeeded in detecting IDV at only 8.6 GHz. PKS 1622–297 had the highest mean linear polarization at 4.8 GHz of the 21 sources in the sample, 5.3%, with similar percentage linear polarization at 8.6 GHz. The on-axis and linear polarization feed design of the ATCA also enables accurate measurements of circular polarization (Rayner et al. 2000), and we note significant levels of circularly polarized radio emission were detected from PKS 1622–297. At 4.8 GHz, a circularly polarized flux density, averaged over three epochs, of -4.8 mJy was detected, corresponding to a fractional circular polarization of -0.16% (the negative sign indicating left-handed polarization).

A number of models have been proposed for the origin of circular polarization, ranging from intrinsic processes to propagation effects (see, e.g., Rayner et al. 2000). Given

the detection of IDV in PKS 1622–297, the model for scintillation-induced circular polarization is of particular interest (Macquart, Melrose 2000). Significant IDV was also observed for PKS 1622–297 in Stokes Q and U , however we limit our discussion here to the IDV in the total flux density.

4. Discussion

4.1. Estimation of Brightness Temperature, Doppler Factor, and Jet Viewing Angle

From the model fitting parameters we can calculate the source brightness temperature in the source’s rest frame, T_B , as

$$T_B = 1.41 \times 10^9 (1+z) (\theta_{\text{maj}} \theta_{\text{min}})^{-1} S \lambda^2 \text{ K}, \quad (1)$$

where θ_{maj} and θ_{min} are the FWHM sizes of the component in the major and minor axes in mas, S is the flux density of the Gaussian component in Jy, and λ is the observation wavelength in centimeters. The brightness temperature of each component is given in table 1. The brightest component C has $T_B = (3.73 \pm 0.07) \times 10^{11}$ K.

The upper limit of the observed brightness temperature is caused by inverse Compton catastrophe (Kellermann, Pauliny-Toth 1969). Using formulae (1a) and (1b) in Readhead (1994), the inverse Compton scattering limit can be calculated as $T_{B,\text{ic}} = 1.02 \times 10^{11}$ K. To derive this, we adopt a synchrotron peak frequency, ν_{peak} , of 43 GHz, a spectral index of -0.7 and assume a synchrotron high-frequency cutoff of 10^4 GHz. Jorstad et al. (2001a) report that the component A, assuming as a core, has an inverted spectrum between 15.4, 22.2 and 43.2 GHz from the simultaneous VLBA observations. On the other

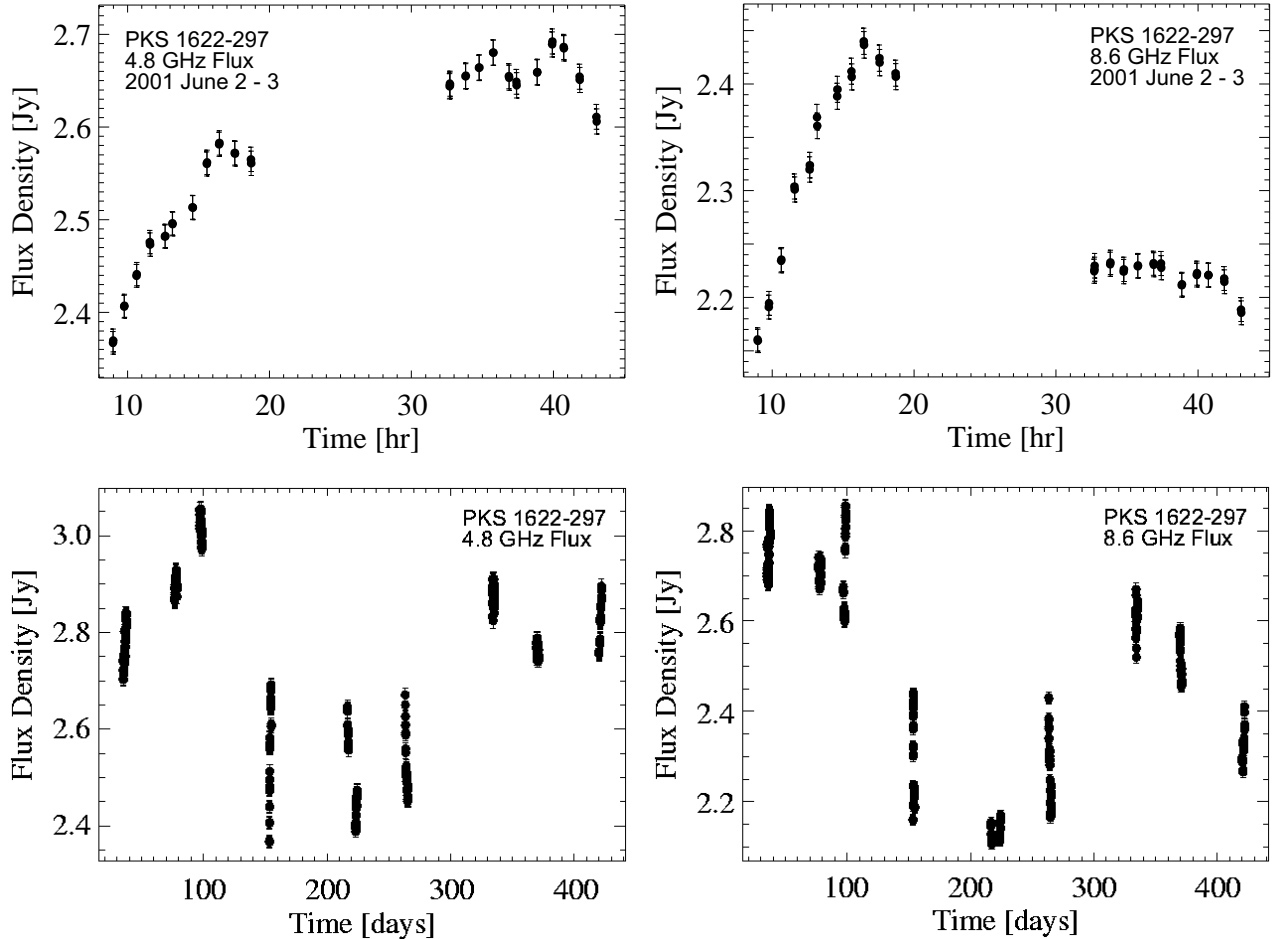


Fig. 5. Results of the flux density monitoring in the ATCA IDV survey program at 4.8 and 8.6 GHz. (Top) Total flux density at 4.8 GHz (left) and 8.6 GHz (right) on 2001 June 2–3, when the largest amplitude IDV was observed. Horizontal axis shows hours UT since 2001 June 2 (day 153), 00:00. (Bottom) Long-term flux variation at 4.8 GHz (left) and 8.6 GHz (right). Horizontal axis shows days since 2001 January 1.

hand, 88, 150, and 230 GHz single-dish measurements at the IRAM 30 m telescope (Steppe et al. 1993; Reuter et al. 1997) show that the source has optically thin spectrum at these frequencies and the flux densities are lower than that at 43 GHz by VLBA (see figure 6). We compiled these results and obtained ν_{peak} and α , although each observation was made at a different epoch. In addition, we adopt a similar value of the synchrotron high-frequency cutoff obtained in the gamma-ray loud quasar 3C 279 (Piner et al. 2003). To reconcile with our T_{B} , a Doppler factor, δ_{ic} , of 2.45 ± 0.05 is required. Here a factor of 0.67 has been used to convert the value of T_{B} , derived assuming a Gaussian component, to that for an optically thin uniform sphere (Marscher 1987). The equipartition brightness temperature limit, $T_{\text{B,eq}}$ can also be estimated assuming the particles and magnetic field are in equipartition (Readhead 1994). In PKS 1622–297, $T_{\text{B,eq}} = 1.03 \times 10^{11} h^{-0.12} \delta_{\text{eq}}^{0.84}$ K. From our observation we derive δ_{eq} as $(2.87 \pm 0.07) h^{0.14}$. Although the obtained δ_{eq} is slightly higher than δ_{ic} , it seems that the core region of PKS 1622–297 is not far from equipartition at this

epoch, in contrast with the results for several other core-dominated sources from VSOP observations (NRAO 530, Bower, Backer 1998; PKS 1921–293, Shen et al. 1999; PKS 1741–038, Wajima et al. 2000).

The viewing angle, ϕ , can be obtained using β_{app} and δ as

$$\phi = \tan^{-1} \frac{2\beta_{\text{app}}}{\beta_{\text{app}}^2 + \delta^2 - 1} \quad (2)$$

(Ghisellini et al. 1993). If each jet component has the same δ as the nucleus we can obtain ϕ of the components by adopting δ_{ic} , as 23.3 ± 0.7 (for B2+D2+E3), 13.2 ± 0.6 (for J2), and 6.9 ± 1.1 (for J1), assuming $h = 0.75$.

The derived δ and ϕ of each component are rather different from other gamma-ray loud AGNs. Especially, δ and ϕ for PKS 1622–297 are very different from PKS 0528+134 ($\delta \gtrsim 15$, $\phi \sim 4^\circ$, Peng et al. 2001) and 3C 279 ($\delta \gtrsim 20$, $\phi \lesssim 4^\circ$, Piner et al. 2003; Jorstad et al. 2004), which show extremely high maximum gamma-ray fluxes of more than 400 pJy (Hartman et al. 1999). As mentioned in section 1, inverse Compton scattering theory (e.g., Sikora et al. 1994) requires a small jet viewing angle

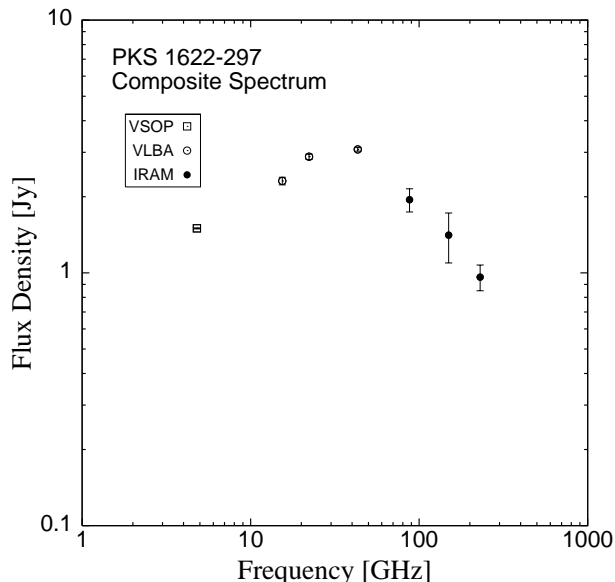


Fig. 6. Composite radio spectrum of PKS 1622–297. Data are from Jorstad et al. (2001a) (VLBA), Reuter et al. (1997) (IRAM), and this work (VSOP). The figure refers only to the flux density of the core component at each frequency. The data are not obtained simultaneously.

for the detection of gamma-ray emission in AGN. Previous theoretical studies imply that objects having larger viewing angles, $\gtrsim 10^\circ$, would be less likely identified as gamma-ray sources (e.g., Dermer 1995; Arbeiter et al. 2002). We cannot conclusively explain from our observation results that the gamma-ray emission from this source is caused by inverse Compton scattering by relativistic electrons in the parsec-scale jet because the ϕ and δ of each component, especially components B2+D2+E3 and J2, are incompatible with other sources. On the other hand, Jiang, Cao, and Hong (1998) report three gamma-ray emitting sources which have larger viewing angles and lower Doppler factors: 0716+714 ($\phi = 44.9^\circ$, $\delta = 1.4$), Mrk 421 ($\phi = 35.2^\circ$, $\delta = 1.3$), and 1219+285 ($\phi = 24.8^\circ$, $\delta = 2.1$). Further VLBI observations are needed for PKS 1622–297 and these three sources, and further consideration as to whether it is possible to detect significant gamma-ray emission from AGNs having such large viewing angles.

It is apparent in figure 4 that the large gamma-ray flare in 1995.48 occurs soon after the (extrapolated) ejection of component B2+D2+E3 from the core, a coincidence also noted by Jorstad et al. (2001a). Romanova and Lovelace (1997) developed a dynamical model of gamma-ray flares and VLBI outbursts of AGNs taking the gamma-ray emission by inverse Compton scattering into account. They applied their model to PKS 1622–297, fitting the calculated light curve to that of the gamma-ray flare in 1995.48 observed by EGRET (Mattox et al. 1997), and determined ϕ to be 5.7° . This is much smaller than ϕ of component B2+D2+E3 obtained from β_{app} and δ_{ic} . Acceptance of their model would then suggest the assumption that each jet component has the same δ as the nucleus is not completely valid.

Our observation reveals that PKS 1622–297 possesses somewhat different features to other gamma-ray emitting AGNs. However, the relatively low brightness temperature we measure may reflect the fact that the source was in a relatively quiescent state at this epoch. A similar conclusion was drawn by Nakagawa et al. (2005) from their VSOP observations of NRAO 530. To reveal the details of the inner region of gamma-ray loud AGN, observations at a mm-wavelength and higher angular resolution VLBI will be essential. There are a number of future VLBI projects that will have the capability of mm-wavelength and higher angular resolution observations, such as the Korean VLBI Network (KVN; Minh et al. 2003) and the next Space VLBI mission (VSOP-2; Hirabayashi et al. 2004). The KVN will be furnished with a multichannel receiver system at 22, 43, 86, and 129 GHz and it will be able to provide important information about wideband spectra, especially in the optically thin regime, for each component. Higher angular resolution VLBI observations by VSOP-2 will give conclusive results for the relation between the gamma-ray flare and emergence of the new VLBI jet component at closer region to the central engine. Especially, VSOP-2 would be able to make observations in conjunction with the GLAST gamma-ray spacecraft (Burnett et al. 2002), which will provide much improved angular resolution and sensitivity ($< 6 \times 10^{-9}$ counts $\text{cm}^{-2} \text{s}^{-1}$ for a point source) compared to EGRET. This will enable the above subject to be clarified.

4.2. Intraday Variability

In the ATCA 2001 June 2 observation, rapid flux density variations of $\sim 12\%$ at both 4.8 and 8.6 GHz were detected within the first eight hours (see the upper panels of figure 5). If the observed flux density variations are intrinsic to the source, the variability brightness temperature, $T_{\text{B,var}}$, can be calculated as $\sim 10^{19} h^{-2}$ K. This would require a Doppler factor at least two orders of magnitude higher than estimated in section 4.1 from the VSOP data for the intrinsic brightness temperature to remain below the inverse Compton scattering limit, implying an intrinsic origin for the IDV is highly unlikely.

As mentioned in section 1, current radio observations show that ISS is mainly responsible for the rapid IDV features. We use the NE2001 Galactic electron density model (Cordes, Lazio 2002) to investigate the likely effect of ISS. The model predicts a transition frequency between weak and strong scattering of 31.7 GHz on the line of sight to PKS 1622–297 (Galactic coordinates $l = 348.8^\circ$, $b = 13.3^\circ$). In this case the observed frequencies would be in the strong scattering regime. The very rapid IDV observed in a few sources has been shown to be due to weak scattering at frequencies $\gtrsim 5$ GHz, in very nearby turbulence (Dennett-Thorpe, de Bruyn 2000; Rickett et al. 2002; Bignall et al. 2003b). However the IDV seen in PKS 1622–297 has a characteristic timescale longer than a day. Our two-day ATCA observations do not provide a sufficient sample of the variability pattern to estimate the characteristic timescale accurately. In many epochs we observe only a steady increase or decrease in flux density.

Even for the most extreme variations observed, in 2001 June as shown in figure 5, the variability pattern is not well-sampled. A characteristic timescale of several days is consistent with refractive interstellar scintillation (RISS) in the strong scattering regime as would be expected at 4.8 and 8.6 GHz for a source along this line of sight through the Galaxy.

If the transition frequency is close to 30 GHz, as expected from the NE2001 model, then applying the theory of strong scattering (Walker 1998) we would expect to see rms modulations of $m \approx 35\%$ at 4.8 GHz and $m \approx 50\%$ at 8.6 GHz for a source of angular size θ_s smaller than the scattering disk θ_{ref} . If $\theta_s > \theta_{\text{ref}}$, then the modulation index will be reduced and the scintillation timescale increased by a factor $\sim \theta_s/\theta_{\text{ref}}$. The NE2001 model predicts scattering disk sizes of 0.16 mas at 4.8 GHz and 0.04 mas at 8.6 GHz for the line of sight to PKS 1622–297. The fitted angular size of component C from the 5 GHz VSOP data is then 3–4 times larger than the predicted scattering disk, we could therefore expect to see rms modulations of order 10% or ~ 150 mJy in this component as a result of RISS. The expected characteristic timescale would be of order one week, depending on the transverse bulk velocity of the scattering plasma with respect to the observer. It may also be the case that some fraction of the flux density of component C is in an even more compact component that is unresolved on VLBI scales, so that this would scintillate on a shorter timescale than the more extended component. After taking into account that PKS 1622–297 has significant flux density, ~ 1 Jy, which is extended on mas to arcsecond scales, the rms variations observed in the ATCA data remain somewhat lower in amplitude than expected from the RISS model. However, since we do not fully sample the scintillation pattern in the ATCA observations, the modulation index is almost certainly underestimated. We conclude that the IDV observed in ATCA data is consistent with what is expected due to RISS of the core component in PKS 1622–297.

As RISS is a stochastic process, sampling of the variability over many more days would be required to accurately estimate the rms flux density variations and characteristic timescales. However, on longer timescales this source is also likely to show intrinsic variability which may complicate analysis.

With the addition of PKS 1622–297, short timescale variability within a few hours to a few days at cm-wavelengths has been reported in 28 sources (42%) of 67 EGRET-identified AGNs to date (Quirrenbach et al. 1992; Wagner, Witzel 1995; Kedziora-Chudczer et al. 2001; and references therein). This compares with a general incidence for IDV among flat-spectrum radio sources of between 10 and 20% (e.g., Kedziora-Chudczer et al. 2001; Lovell et al. 2003), suggesting a higher incidence of IDV among gamma-ray sources, a possibility which has been noted previously (Wagner, Witzel 1995). If the IDV is due to ISS, each source should have a compact core between several tens to a few hundred μas , corresponding to a linear scale of about 10^{17} cm, depending on the source’s distance. This linear scale of the core is simi-

lar to, or slightly larger than, those obtained by Sikora et al. (1997), assuming an external radiation Compton model (e.g. Sikora et al. 1994) can account for the gamma-ray emission. Again, the VSOP-2 mission will enable the inner region of the core to be observed with a maximum angular resolution of $38 \mu\text{as}$, comparable to the linear scale of the gamma-ray emission region. VSOP-2 would certainly be able to tell us more about how the core flux density is distributed and would allow us to measure scatter-broadening in sources which are moderately strongly scattered.

5. Conclusions

We have observed the gamma-ray loud quasar PKS 1622–297 using the HALCA satellite and three ground radio telescopes. The source was clearly resolved and we could determine three distinct features, the core and two jet components, and have confirmed that both jet components display superluminal motion. By using the inverse Compton catastrophe model we estimated the Doppler factor, δ , as 2.45, and the jet viewing angle, ϕ , of each component as larger than $6^\circ.9$. Especially, the innermost component has very large viewing angle, $\phi = 23^\circ.3$. Both δ and ϕ are rather different from other gamma-ray loud AGNs yet observed, though this may be due to the quasar being in a relatively quiescent (i.e., low brightness temperature) state during the epoch of the VSOP observation. Although some previous theoretical and observational studies have implied the possibility of inverse Compton scattering as the gamma-ray emission mechanism, the VSOP observations at epoch 1998.15 do not on their own provide any supporting evidence.

We have also presented the results of the ATCA total flux density monitoring between February 2001 and February 2002. PKS 1622–297 displays IDV at both 4.8 and 8.6 GHz throughout this year. The extremely high brightness temperature implied for the IDV being due to fluctuations intrinsic to the source strongly favor refractive interstellar scintillation as the origin of the IDV.

In either case, compact structure at a level significantly below the angular resolution of our VSOP observations can be inferred. Scattering models imply the existence of a compact core, ~ 0.1 mas in angular size, or $\sim 10^{17}$ cm in linear size. This is comparable to the gamma-ray emitting region expected from the theoretical model.

We are grateful to the referee, Dr. David L. Jauncey, for valuable comments which improved the manuscript. We gratefully acknowledge the VSOP Project, which is led by the Japanese Institute of Space and Astronautical Science of the Japan Aerospace Exploration Agency in cooperation with many organizations and radio telescopes around the world. Especially, we acknowledge three ground telescopes, Hartbeesthoek, Hobart, and Shanghai, for participating the VSOP observation. The research was carried out using an observation of the VSOP Survey Program. The research has made use of data from the University of Michigan Radio Astronomy Observatory which has been

supported by the University of Michigan and the National Science Foundation. The Australia Telescope Compact Array is part of the Australia Telescope which is funded by the Commonwealth of Australia for operation as a National Facility managed by CSIRO. KW acknowledges support from Korea Science and Engineering Foundation (KOSEF).

References

- Arbeiter, C., Pohl, M., & Schlickeiser, R. 2002, *A&A*, 386, 415
- Balbi, A., et al. 2000, *ApJ*, 545, L1 (erratum 2001, 558, L145)
- Bignall, H. E. 2003a, PhD Thesis, University of Adelaide
- Bignall, H. E., et al. 2003b, *ApJ*, 585, 653
- Bower, G. C., & Backer, D. C. 1998, *ApJ*, 507, L117
- Burnett, T. H., & GLAST Team 2002, *BAAS*, 34, 1315
- Carlson, B. R., Dewdney, P. E., Burgess, T. A., Casorso, R. V., Petrachenko, W. T., & Cannon, W. H. 1999, *PASP*, 111, 1025
- Cordes, J. M., & Lazio, T. J. W. 2002, astro-ph/0207156
- Dennett-Thorpe, J., & de Bruyn, A. G. 2000, *ApJ*, 529, L65
- Dermer, C. D. 1995, *ApJ*, 446, L63
- Fomalont, E. B., Frey, S., Paragi, Z., Gurvits, L. I., Scott, W. K., Taylor, A. R., Edwards, P. G., & Hirabayashi, H. 2000, *ApJS*, 131, 95
- Ghisellini, G., Padovani, P., Celotti, A., & Maraschi, L. 1993, *ApJ*, 407, 65
- Hartman, R. C., et al. 1999, *ApJS*, 123, 79
- Hirabayashi, H., et al. 1998, *Science*, 281, 1825 (erratum 1998, 282, 1995)
- Hirabayashi, H., et al. 2000, *PASJ*, 52, 997
- Hirabayashi, H., et al. 2004, *Proc. SPIE*, 5487, 1646
- Impey, C. D., & Tapia, S. 1990, *ApJ*, 354, 124
- Jackson, C. A., Wall, J. V., Shaver, P. A., Kellermann, K. I., Hook, I. M., & Hawkins, M. R. S. 2002, *A&A*, 386, 97
- Jauncey, D., L., Bignall, H. E., Lovell, J. E. J., Kedziora-Chudczer, L., Tzioumis, A. K., Macquart, J. -P., & Rickett, B. J. 2003, in *ASP Conf. Ser. 300, Radio Astronomy at the Fringe*, ed. J. A. Zensus, M. H. Cohen, & E. Ros (San Francisco: ASP), 199
- Jauncey, D., L., & Macquart, J. -P. 2001, *A&A*, 370, L9
- Jiang, D. R., Cao, X., & Hong, X. 1998, *ApJ*, 494, 139
- Jorstad, S. G., Marscher, A. P., Lister, M. L., Stirling, A. M., Cawthorne, T. V., Gómez, J. -L., & Gear, W. K. 2004, *AJ*, 127, 3115
- Jorstad, S. G., Marscher, A. P., Mattox, J. R., Aller, M. F., Aller, H. D., Wehrle, A. E., & Bloom, S. D. 2001b, *ApJ*, 556, 738
- Jorstad, S. G., Marscher, A. P., Mattox, J. R., Wehrle, A. E., Bloom, S. D., & Yurchenko, A. V. 2001a, *ApJS*, 134, 181
- Kedziora-Chudczer, L. L., Jauncey, D. L., Wieringa, M. H., Tzioumis, A. K., & Reynolds, J. E. 2001, *MNRAS*, 325, 1411
- Kellermann, K. I., & Pauliny-Toth, I. I. K. 1969, *ApJ*, 155, L71
- Königl, A. 1981, *ApJ*, 243, 700
- Lovell, J. E. J., Jauncey, D. L., Bignall, H. E., Kedziora-Chudczer, L., Macquart, J. -P., Rickett, B. J., & Tzioumis, A. K. 2003, *AJ*, 126, 1699
- Macquart, J. -P., & Melrose, D. B. 2000, *ApJ*, 545, 798
- Marscher, A. P. 1987, in *Superluminal Radio Sources*, ed. J. A. Zensus & T. J. Pearson (Cambridge and New York: Cambridge University Press), 280
- Mattox, J. R., Wagner, S. J., Malkan, M., McGlynn, T. A., Schachter, J. F., Grove, J. E., Johnson, W. N., & Kurfess, J. D. 1997, *ApJ*, 476, 692
- Minh, Y. C., Roh, D. -G., Han, S. -T., & Kim, H. -G. 2003, in *ASP Conf. Ser. 306, New Technologies in VLBI*, ed. Y. C. Minh (San Francisco: ASP), 373
- Nakagawa, A., Edwards, P. G., Murata, Y., Wajima, K., & Omodaka, T. 2005, *PASJ*, 57, 295
- Peng, B., et al. 2001, *ApJ*, 551, 172
- Piner, B. G., Unwin, S. C., Wehrle, A. E., Zook, A. C., Urry, C. M., & Gilmore, D. M. 2003, *ApJ*, 588, 716
- Quirrenbach, A., et al. 1992, *A&A*, 258, 279
- Rayner, D. P., Norris, R. P., & Sault, R. J. 2000, *MNRAS*, 319, 484
- Readhead, A. C. S. 1994, *ApJ*, 426, 51
- Reuter, H. -P., et al. 1997, *A&AS*, 122, 271
- Rickett, B. J., Witzel, A., Kraus, A., Krichbaum, T. P., & Qian, S. J. 2001, *ApJ*, 550, L11
- Rickett, B. J., Kedziora-Chudczer, L., & Jauncey, D. L. 2002, *ApJ*, 581, 103
- Romanova, M. M., & Lovelace, R. V. E. 1997, *ApJ*, 475, 97
- Saikia, D. J., Singal, A. K., & Cornwell, T. J. 1987, *MNRAS*, 224, 379
- Sault, R. J., Teuben, P. J., & Wright, M. C. H. 1995, in *ASP Conf. Ser. 77, Astronomical Data Analysis Software and Systems IV*, ed. R. A. Shaw, H. E. Payne, & J. J. E. Hayes (San Francisco: ASP), 433
- Shen, Z. -Q., Edwards, P. G., Lovell, J. E. J., Fujisawa, K., Kameno, S., & Inoue, M. 1999, *PASJ*, 51, 513
- Shepherd, M. C. 1997, in *ASP Conf. Ser. 127, Astronomical Data Analysis Software and Systems VI*, ed. G. Hunt & H. E. Payne (San Francisco: ASP), 77
- Sikora, M., Begelman, M. C., & Rees, M. J. 1994, *ApJ*, 421, 153
- Sikora, M., Madejski, G., Moderski, R., & Poutanen, J. 1997, *ApJ*, 484, 108
- Sowards-Emmerd, D., Romani, R. W., & Michelson, P. F. 2003, *ApJ*, 590, 109
- Sowards-Emmerd, D., Romani, R. W., Michelson, P. F., & Ulvestad, J. S. 2004, *ApJ*, 609, 564
- Steppe, H., et al. 1993, *A&AS*, 102, 611
- Stickel, M., Meisenheimer, K., & Kühr, H. 1994, *A&AS*, 105, 211
- Tabara, H., & Inoue, M. 1980, *A&AS*, 39, 379
- Tingay, S. J., Jauncey, D. L., King, E. A., Tzioumis, A. K., Lovell, J. E. J., & Edwards, P. G. 2003, *PASJ*, 55, 351
- Tingay, S. J., Murphy, D. W., & Edwards, P. G. 1998, *ApJ*, 500, 673
- Tingay, S. J., et al. 2002, *ApJS*, 141, 311
- Wagner, S. J., & Witzel, A. 1995, *ARA&A*, 33, 163
- Wajima, K., Lovell, J. E. J., Kobayashi, H., Hirabayashi, H., Fujisawa, K., & Tsuboi, M. 2000, *PASJ*, 52, 329
- Walker, M. A. 1998, *MNRAS*, 294, 307
- Wright, A., & Otrupcek, R. 1990, *Parkes Catalogue*, Australia Telescope National Facility, CSIRO